Molecular Therapy
Oncolytics
Original Article

Boosting antitumor response with PSMA-targeted immunomodulatory VLPs, harboring costimulatory TNFSF ligands and GM-CSF cytokine

Soledad Palameta,[1,2] Andrea J. Manrique-Rincón,[1,4] Jessica M. Toscaro,[1,4] Isadora F. Semionatto,[1,3] Matheus C. Fonseca,[1,2] Rhubia S.M. Rosa,[1,3] Luciana P. Ruas,[1] Paulo S.L. Oliveira,[1,2] and Marcio C. Bajgelman[1,3,4]

[1]Brazilian Biosciences National Laboratory, Center for Research in Energy and Materials, Campinas, SP, Brazil; [2]Institute of Biology, University of Campinas, Campinas, SP, Brazil; [3]Faculty of Pharmaceutical Sciences, University of Campinas, Campinas, SP, Brazil; [4]University of Campinas Medical School, Campinas, SP, Brazil

Therapeutic strategies based on immunomodulation have improved cancer therapy. Most approaches target co-stimulatory pathways or the inhibition of immunosuppressive mechanisms, to enhance immune response and overcome the immune tolerance of tumors. Here, we propose a novel platform to deliver targeted immunomodulatory signaling, enhancing antitumor response. The platform is based on virus-like particles derived from lentiviral capsids. These particles may be engineered to harbor multifunctional ligands on the surface that drive tropism to the tumor site and deliver immunomodulatory signaling, boosting the antitumor response. We generated virus-like particles harboring a PSMA-ligand, TNFSF co-stimulatory ligands 4-1BBL or OX40L, and a membrane-anchored GM-CSF cytokine. The virus-like particles are driven to PSMA-expressing tumors and deliver immunomodulatory signaling from the TNFSF surface ligands and the anchored GM-CSF, inducing T cell proliferation, inhibition of regulatory T cells, and potentiating elimination of tumor cells. The PSMA-targeted particles harboring immunomodulators enhanced antitumor activity in immunocompetent challenged mice and may be explored as a potential tool for cancer immunotherapy.

INTRODUCTION

The therapeutic strategies targeting antitumor immunity have shown remarkable clinical results. However, there are still numerous cases of resistant tumors and therefore the need to explore new antitumor approaches.[1–3] Most of the immunomodulatory strategies that are currently being pursued in clinics target checkpoint inhibition,[4–6] while other approaches may also aim at co-stimulating lymphocyte receptors, such as 4-1BB (CD137) and OX40 (CD134) expressed on the surface of T cells, inducing agonist phenotypic changes in addition to contributing to the inhibition of immunosuppressive mechanisms associated with tumor cell tolerance.[7–9]

The co-stimulatory signaling driven to 4-1BB receptor promote survival, clonal expansion, and strengthening of T cell activation, inducing the elimination of tumors in animals.[10–12] The agonist anti-4-1BB monoclonal antibody exhibits co-stimulatory activity and has been used in clinical trials.[13] Agonist antibodies driven to the OX40 receptor may also co-stimulate T cells, enhancing activation and inducing lymphocyte proliferation. The co-stimulation of OX40 may increase the longevity of T cells, and clinical data suggest that lymphocytic infiltrates that have high OX40 expression are correlated with a lower incidence of metastases and a better prognosis for patients.[14,15] Literature data also demonstrate that agonist antibodies for the co-stimulation of OX40 expressed in regulatory T cells may inhibit the expression of FoxP3 transcription factor, which is associated with the maintenance of the immunosuppressive regulatory T cell (Treg) phenotype.[16,17] The antitumor T cell activity may be enhanced by combining other additive stimuli as provided by the granulocyte-macrophage colony-stimulating factor (GM-CSF) cytokine, which plays an important role in dendritic cell (DC) maturation, increasing the presentation of tumor antigens to the immune system.[18,19]

The generation of monoclonal antibodies requires a relatively complex approach, involving the immunization of animals and the selection of producer clones and establishment of lineages. In this sense, as an alternative to monoclonal antibodies, there are efforts being made to develop other molecules, for example, based on the use of soluble ligands or agonist aptamers.[20–23] We have recently demonstrated that extracellular vesicles (EVs) produced by antitumor vaccines harboring tumor necrosis factor superfamily 4-1BBL and OX40L may exhibit immunomodulatory activity, stimulating antitumor effects *in vitro*.[24] These vesicles represent a heterogeneous population composed of microvesicles and exosomes. The microvesicles themselves are particles from 50 to 1,000 nm in diameter that are formed by the shedding of the plasma membrane.[25] Exosomes are formed by the fusion of the multivesicular endosome with the plasma membrane, generating particles of approximately 40–100 nm in

Received 23 September 2021; accepted 11 February 2022;
https://doi.org/10.1016/j.omto.2022.02.010.

Correspondence: Marcio Bajgelman, PhD, Brazilian Biosciences National Laboratory, Center for Research in Energy and Materials, Campinas, SP, Brazil.
E-mail: marcio.bajgelman@lnbio.cnpem.br

diameter.[25] Enveloped virus-like particles (VLPs) derived from retroviruses are formed in a manner similar to that of exosomes.[26,27] VLPs are structurally well defined, harboring virus capsid and lacking the genome. Due to the high plasticity of VLPs, it is possible to load a cargo or even decorate its surface with peptide ligands or other recombinant proteins, using these VLPs as delivery tools for enhancing the immune response.[28–30] Some studies propose the use of VLPs for the development of antitumor strategies. These particles may be targeted to tumor sites by functionalizing their surfaces with ligands.[31–33] The VLPs may be engineered to stimulate immunity against tumors and are being explored as cancer vaccines for cervical cancer, breast cancer, colorectal cancer, pancreatic cancer, and skin cancer, among others.[34–38]

In this work, we propose a new VLP-based platform derived from lentiviral capsids. Lentiviral platforms have been explored since the 1990s and are considered to be highly plastic and safe.[39,40] The lentiviral-derived particles may be pseudotyped with heterologous envelope to drive tropism to specific tissues.[39,41,42] Our aim was to engineer VLPs derived from lentiviral capsids that specifically bind to tumor cells that have the prostate-specific membrane antigen receptor (PSMA) and deliver immunomodulatory signaling to stimulate antitumor responses.

The PSMA receptor is upregulated in prostate cancer cells, and several studies also have shown PSMA expression in the tumor-associated vasculature of other tumor types, such as breast cancer, lung cancer, bladder cancer, brain cancer, and gastric cancer.[43–49] The VLP capsid is decorated with peptide sequences originated from a phage display library,[50] therefore driving VLP to the PSMA-positive cells at the tumor site. In addition, we have decorated the VLP surface with co-stimulatory TNFSF ligands 4-1BBL, OX40L, and a membrane-bound GM-CSF. In this way, the multifunctional immunomodulatory VLP exhibits tropism for positive PSMA tumor cells and may drive the GM-CSF factor in combination with TNFSF ligands, such as 4-1BBL and OX40L. We have shown the targeted-specific VLPs have a substantial potential for immunomodulation, inducing increased proliferation of T cells and inhibition of Tregs and enhancing the elimination of tumor cells.

RESULTS

Surface-decorated VLPs harboring TNFSF ligands bind to TNFSF receptors

The lentivirus-derived VLPs may be engineered to harbor TNFSF ligands such as 4-1BBL and OX40L. The VLPs are generated in producer cells by co-transfecting an expression vector that encodes a surface ligand (Figure S1) with a packaging vector that encodes the structural proteins of the VLP capsid (Figure S2). The VLP preparation is harvested and purified from the supernatant. The immunomodulatory particles exhibit a typical lentiviral-derived size distribution of approximately 100–200 nm and spherical shaped morphology[51–53] (Figures 1A and 1B). To characterize the presence of both ligands in the 4-1BBL + OX40L bivalent VLPs, we performed flow cytometry assays in which the VLPs were labeled by incubating along previously bound beads and capture antibodies for the first ligand, followed by the detection antibody for the second ligand. The flow cytometry assay revealed anti-4-1BBL or anti-OX40L labeling when the VLPs were captured by anti-OX40L and anti-4-1BBL beads, respectively (Figures 1C and 1D). Since VLPs harbor p24, which is also used as a marker to quantify lentiviral particles,[54,55] we also performed a flow cytometry assay with 4-1BBL VLPs, using anti-p24 capture beads and staining for anti-41BBL (Figure S3). To better characterize the TNFSF ligands on the surface of the bivalent VLP, we performed a cell culture assay to verify whether the ligand on the surface of the VLP could specifically interact with its TNFSF receptor (TNFSFR) expressed on cells. Therefore, we used the 4-1BBL + OX40L bivalent VLP incubated with parental NIH-3T3 cells or with genetically modified NIH-3T3 cells to express the TNFSF 4-1BB receptor. The bivalent VLP harbors the 4-1BBL ligand that specifically binds to the 4-1BB receptor on cells. As the bivalent VLP also harbors OX40L, we could label the bound VLPs with an anti-OX40L antibody labeled with Phycoerythrin (PE). As expected, only 4-1BB receptors expressing NIH-3T3 cells incubated with the 4-1BBL + OX40L bivalent VLPs were labeled with the anti-OX40L PE antibody, in contrast to the control VLPs (lacking surface ligands) (Figures 1E and 1F).

VLPs harboring 4-1BB and OX40 ligands boost T cell activation, induce inhibition of Tregs,s and potentiate the elimination of tumor cells *in vitro*

Agonist antibodies or even soluble TNFSF ligands may potentiate antitumor T cell activity. Therefore, we sought to investigate whether VLPs harboring TNFSF ligands could stimulate lymphocytes. We initially performed a proliferation assay, in which primary T cells were labeled with the carboxyfluorescein succinimidyl ester (CFSE) fluorophore and then incubated with APC cells and VLPs expressing TNFSF ligands. We tested monovalent VLPs harboring only one surface ligand such as OX40L or 4-1BBL and the bivalent VLP harboring simultaneously both 4-1BBL and OX40L. We observed that the monovalent and bivalent VLPs induced increased T cell proliferation and increased interferon (IFN)-gamma secretion in cell culture supernatants, an important biomarker associated with the T helper 1 (Th1) antitumor response and activity of cytotoxic T cells (Figures 2A and S4).

To assess the potential for antitumor immunomodulation of our TNFSF ligands harboring VLPs, we performed an *in vitro* assay in which B16F10 tumor cells were incubated with splenocytes in the presence of these VLPs. The B16F10 tumor cells were genetically modified to express the eGFP reporter gene, enabling a high content imaging analysis. When the VLP-mediated immunomodulation occurs, tumor cells may be lysed by splenocytes and consequently reduce the GFP-positive cell count. Therefore, the number of B16F10-GFP-positive cells were reduced when incubated with splenocytes and treated with VLPs expressing 4-1BB and OX40 ligands compared to the control VLP (Figure 2B).

The literature has demonstrated that an agonist stimulation of the OX40 surface receptor on T cells may induce the inhibition of the

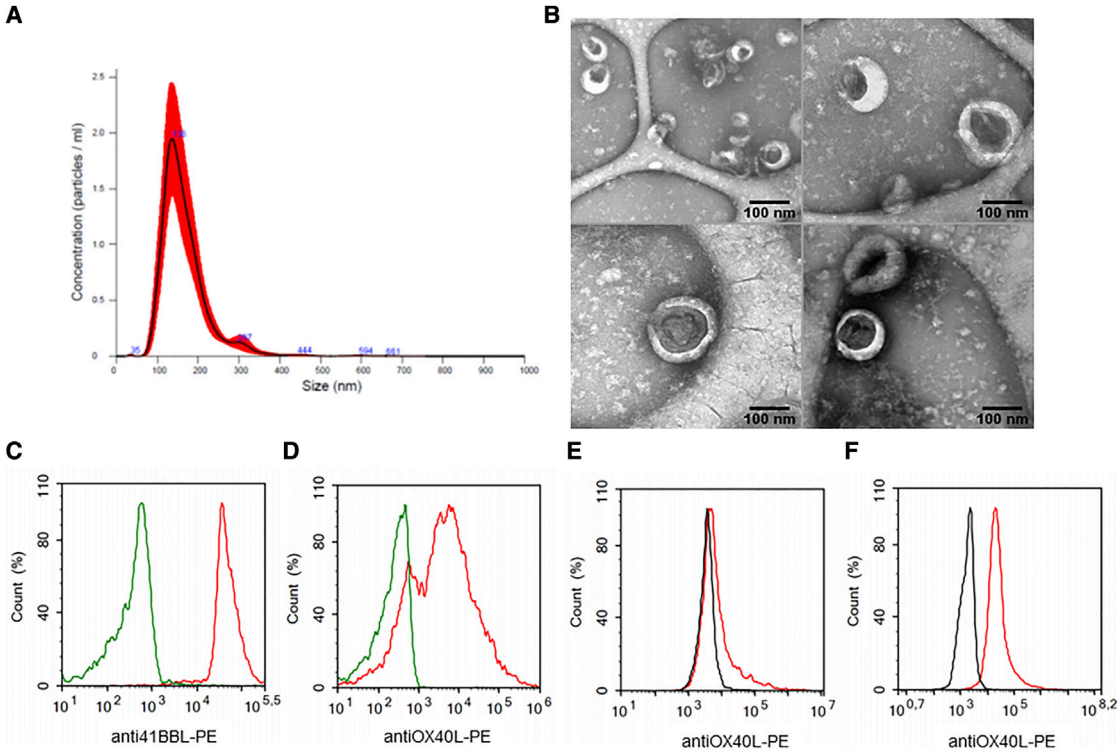

Figure 1. Production and phenotypic characterization of VLPs expressing 4-1BB and OX40 ligands

(A) Size distribution and concentration of the VLPs were analyzed using nanoparticle tracking analysis (NTA). VLPs were purified and concentrated from the supernatant of HEK293T cells co-transfected with 4-1BB and OX40 ligands and analyzed by NTA. The graph is representative of the 4-1BBL + OX40L bivalent VLPs with a size of 136.5 ± 2 nm and a concentration of $1.81 \times 10^{11} \pm 4.82 \times 10^{10}$ particles/mL. Five videos of 30 s per sample, captured at 18°C, were performed for measurement. Particle size and concentration were defined as an average of the videos analyzed. (B) Transmission electron microscopy with negative staining analysis of VLPs. The purified VLPs were adsorbed on copper grids with negative staining with uranyl acetate. VLPs are identified as spherical electrodense structures surrounded by a shiny crown. The panel shows images of transmission electron microscopy acquired for 4 different fields, using 20,000 and 50,000 magnifications. (C and D) TNF ligands anchored in the membrane of the VLPs can be detected by flow cytometry. To check the 4-1BB and OX40 ligands on the surface of the VLPs, polystyrene beads (5×10^4) were previously loaded with a capture antibody for one of the ligands on the VLPs followed by flow cytometry detection with the antibody for the other ligand. Then, anti-4-1BBL (C) or anti-OX40L (D) capture antibodies were absorbed into the beads, which were then incubated with 10^9 particles of the control VLP (green curve; $8.11 \times 10^{11} \pm 1.12 \times 10^{10}$ particles/mL) or 4-1BBL + OX40L bivalent VLP (red curve, $7.64 \times 10^{11} \pm 3.35 \times 10^{10}$). Subsequently, the beads were stained with anti-4-1BBL PE or anti-OX40L PE detection antibodies and flow cytometry was performed. (E and F) Bivalent VLPs exhibit specific binding to the cell surface target receptors. NIH-3T3 cells (black curve) and NIH-3T3-4-1BB cells (red curve), 5×10^4 cells/well, were incubated with 10^9 particles of the control VLP ($8.11 \times 10^{11} \pm 1.12 \times 10^{10}$ particles/mL) (E) or 4-1BBL + OX40L VLP ($7.64 \times 10^{11} \pm 3.35 \times 10^{10}$ particles/mL) (F) and followed by staining with the anti-OX40L PE. Flow cytometry was performed and the data analyzed using the FCS Express 5 software. (C–F) The y axis represents the cell count normalized to a 100% scale and the x axis is the mean fluorescence intensity (MFI) on a logarithmic scale (N = 3).

FoxP3 transcription factor.[17] We have previously observed that EVs harboring OX40L may inhibit FoxP3.[24] In this sense, we investigated the potential of OX40L VLPs to inhibit FoxP3 expression in inducible Tregs (iTR). In this assay, primary cells isolated from C57BL/6 mice were incubated with a Treg induction cocktail containing transforming growth factor (TGF)-beta in the presence of VLPs, and then these cells were stained to evaluate FoxP3-positive cells. As a result, we found that VLPs expressing the OX40 ligand significantly reduced the conversion of FoxP3-positive cells (Figure 2C). Next, we investigated whether the reduction of FoxP3 induced by OX40L VLP would also be correlated to the inhibition of the immunosuppressive phenotype of Treg. For this, we performed a proliferation assay, in which iTR cells previously incubated with VLPs were co-cultured with CFSE-labeled conventional T cells (Tconv). We found that VLPs expressing the OX40 ligand induced a substantial inhibition of the immunosuppressive phenotype of Tregs (Figure 2D).

Immunomodulatory VLPs can be engineered to target PSMA-expressing tumor cells

The administration of agonist mediators by the systemic route may not reach the desired target or may even cause undesired toxicity. Therefore, a target-driven VLP could be used to drive immunomodulatory TNFSF ligands and even anchor soluble molecules such as GM-CSF to tumor cells. We generated trivalent VLPs harboring the LD ligand, a previously described tumor-targeting PSMA ligand,[50] the immunomodulatory TNFSF ligands 4-1BBL or OX40L, and an anchored GM-CSF cytokine. The trivalent VLPs exhibited a similar size distribution, with an average size of 150–160 nm, when compared

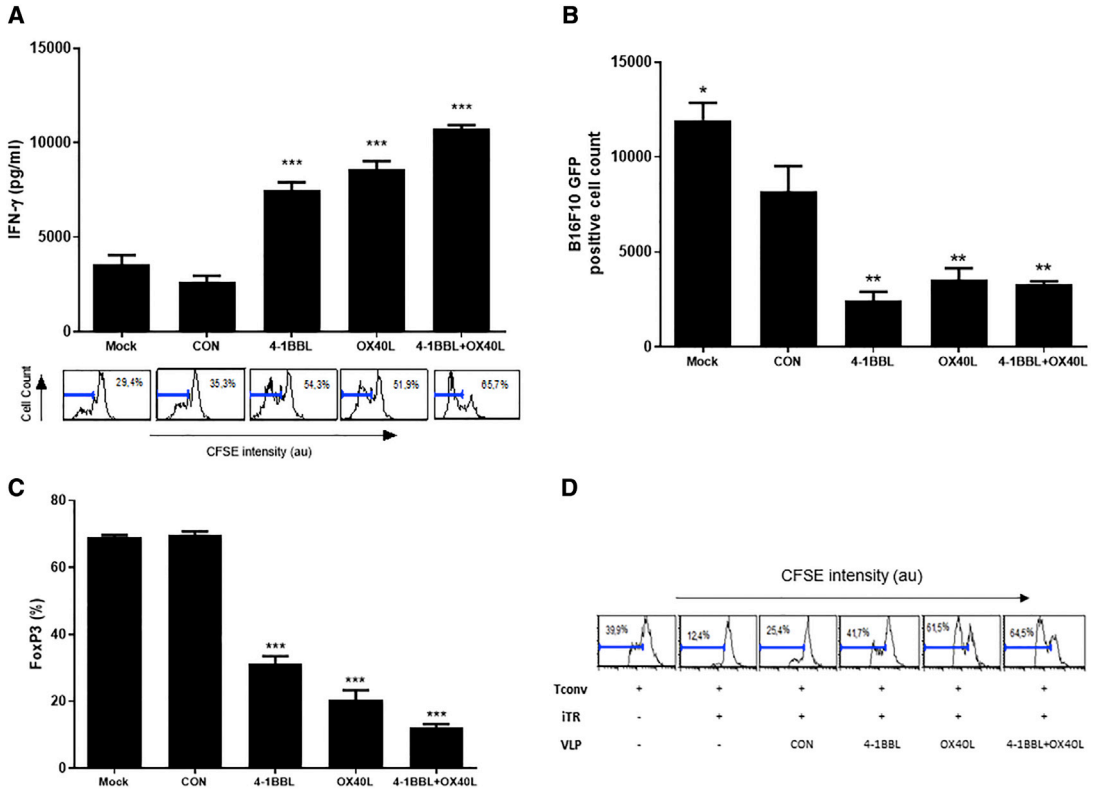

Figure 2. VLPs expressing TNFSF ligands show antitumor immunomodulatory activity

(A) VLPs induce the proliferation of CFSE-labeled CD4 T cells. CD4 T cells isolated from mouse splenocytes were stained with CFSE and plated 5×10^4 cell/well in a 96-well plate and incubated with 5×10^4 APC and 2×10^8 particles from the indicated VLPs. The supernatant from each well was harvested to measure IFN-gamma activity in each condition by ELISA assay. (B) VLPs expressing TNF ligands mediated tumor cell death. T cell-mediated antitumor cytotoxicity assay tumor cells expressing the cytoplasmic marker GFP were incubated with splenocytes in the absence and presence of the VLPs (2×10^8 particles) indicated on the x axis. After 72 h of incubation, positive GFP cell counts were performed, using Operetta equipment (PerkinElmer, Waltham, MA, USA). (C) VLPs harboring TNFSF ligands can inhibit the expression of the transcription factor FoxP3 in regulatory T cells. CD4 T cells (2×10^5 cells) were incubated with an induction cocktail for iTR generation and treated with 5×10^8 particles of the indicated VLPs. The cells were harvested after 48 h and analyzed by flow cytometry to evaluate the expression of FoxP3. (D) VLPs harboring the OX40L ligand show an inhibitory effect on regulatory T cells and stimulate the proliferation of CFSE-labeled conventional T cells. FoxP3 inhibition induced by immunomodulatory VLP attenuates the immunosuppressive phenotype of regulatory T cells. iTR cells (2×10^5 cells) previously treated with 5×10^8 particles of the indicated VLPs were co-cultured with CFSE-labeled conventional CD4 T cells (Tconv) in a 1:8 ratio of iTR:Tconv cells and incubated for 72 h at 37°C. The immunosuppression capacity of iTR cells was determined by inhibiting the proliferation of Tconv cells, indicated by the CFSE intensity decay by flow cytometry. The analysis of all of the data by flow cytometry was performed using the FCS Express 5 software. The samples were performed in triplicate, and each experiment represents 1 of 3 independent experiments. Graphs show the mean and the respective SEM. The p value was calculated using 1-way ANOVA (Dunnett's multiple comparison test) between the control group and treatment groups (*$p < 0.05$, **$p < 0.01$, ***$p < 0.005$, ****$p < 0.0001$e). Mock (absence of VLP), CON (negative control VLP, without ligands; $8.11 \times 10^{11} \pm 1.12 \times 10^{10}$ particles/mL) OX40L (VLP coated with OX40L; $8.56 \times 10^{11} \pm 2.42 \times 10^{10}$ particles/mL), 4-1BBL (VLP coated with 4-1BBL ligand; $3.9 \times 10^{11} \pm 1.38 \times 10^{10}$ particles/mL), and 4-1BBL + OX40L (bivalent VLP, coated with 4-1BBL and OX40L ligands; $1.28 \times 10^{12} \pm 5.04 \times 10^{10}$ particles/mL).

to bivalent VLPs (Figure S5A). The trivalent VLP was analyzed by flow cytometry to confirm the presence of surface TNFSF ligands (4-1BBL or OX40L) and the anchored GM-CSF (Figure S5B). The GM-CSF also could be detected by an ELISA assay (Figure S6).

To investigate whether the LD-VLP was target specific, we performed an *in vitro* assay with PSMA-expressing cells. The B16F10 cells and PSMA-expressing B16F10 cells were incubated with the trivalent VLP LD-GM-CSF-4-1BBL that expresses the PSMA-specific ligand LD, the immunomodulatory 4-1BBL ligand and the GM-CSF anchored cytokine. The cells incubated with VLPs were labeled with anti-4-1BBL and analyzed by confocal microscopy showing that the PSMA-targeted LD-VLPs were bound to the cell surface of PSMA-expressing target cells (Figures 3A and 3B). In addition, we could observe a selective binding of LD-VLPs to PSMA-bound beads, by flow cytometry (Figure S7). The PSMA receptor is a widely explored target in therapeutic approaches because it allows the internalization of small molecules such as antibodies and aptamers.[56,57] To better assess whether particles could be internalized by the PSMA receptor, we generated lentiviral preparations encoding the GFP reporter and decorated with the LD ligand envelope. These GFP-lentivector preparations, containing 10^5 particles, were incubated with

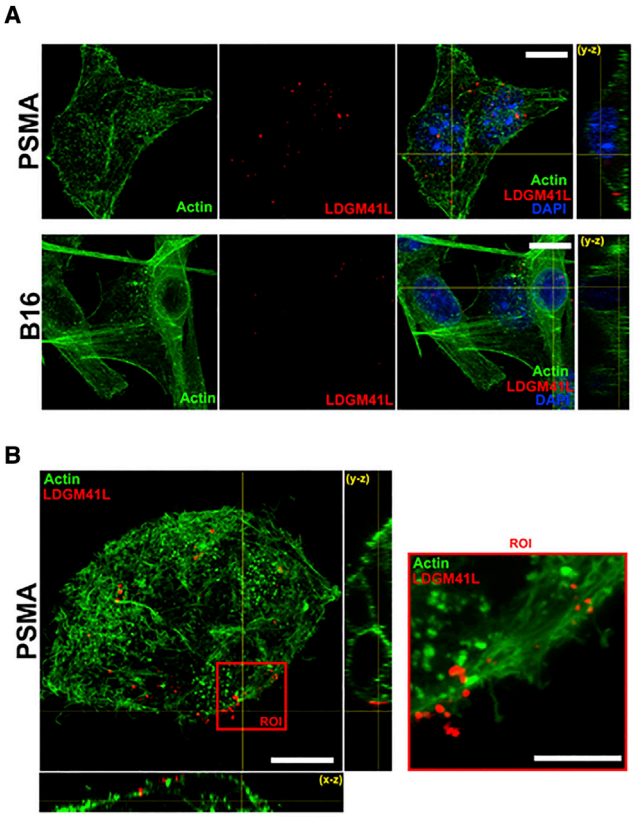

Figure 3. LD-VLP binds to PSMA target cell

Confocal microscopy images of B16F10 and B16F10-PSMA cells (3×10^5 cells) incubated with LD + GM-CSF + 4-1BBL VLPs (3×10^8 particles; $1.12 \times 10^{13} \pm 1.58 \times 10^{12}$ particles/mL) and labeled with anti-4-1BBL antibody. (A) Orthogonal view of plans (y-z) shows the VLPs staining on the surface of PSMA-positive target cells but parental B16F10 cells. The beta-actin cytoskeleton staining is shown in green, nuclei are shown in blue, and VLPs are visualized in red (scale bar: 10 μm). (B) Stimulated emission depletion (STED) microscopy imaging of PSMA-positive cluster of cells stained for beta-actin cytoskeleton (green) and VLPs (red). The region of interest (ROI) exhibits STED imaging. The orthogonal view of the plans (x-z and y-z) show the VLPs staining (red) on the surface of target cells (scale bar, 5μm).

parental B16 cells or B16-PSMA for 48 h followed by flow cytometry analysis of the cells. We used as a positive control the same GFP reporter lentivirus (10^5 particles), decorated with a VSV-G[58] heterologous envelope, which is typically used in lentiviral vectors. The result of the experiment can be seen in Figure S8, where we did not observe significant levels of cells transduced with LD-lentivector compared to VSV-G-lentivector.

The trivalent VLP harboring LD + GM-CSF + TNFSF ligands also induced inhibition in FoxP3 CD4 T cell conversion, as previously observed for bivalent VLP LD + TNFSF ligands (Figure 4A). To evaluate the activity of the anchored GM-CSF, the trivalent GM-CSF VLPs were incubated with mouse bone marrow cells under interleukin-4 (IL-4) stimulation to generate (DCs). The induced DCs were harvested and stained for typical markers such as CD11c, major histocompatibility complex (MHC) class II and CD86.[59,60] It was observed that both LD+GM-CSF+4-1BBL and LD+GM-CSF+OX40L induced the upregulation of MHC class II and CD86 (Figure 4B). It was interesting to note that the membrane GM-CSF content per 5×10^9 particles was estimated in 2.5 ng/mL (Figure S6). Even with this lower membrane GM-CSF content compared to the recombinant GM-CSF concentration, we could observe a comparable effect on DC generation.

Immunomodulatory VLPs boost antitumor response in challenged mice

To explore the *in vivo* impact of immunomodulatory VLPs, we performed experiments with C57/BL6 immunocompetent animals, which were subcutaneously challenged with syngeneic B16F10-expressing PSMA tumor cells. The VLPs were given by intraperitoneal injection. The tumor growth was monitored to evaluate the antitumor activities of the VLPs. We initially compared the efficiency of two VLPs configuration, the LD + GM-CSF + 4-1BBL and the LD + GM-CSF + OX40L. The combination LD + GM-CSF + OX40L was slightly more efficient to inhibit tumors when compared to the LD + GM-CSF + 4-1BBL VLP (Figures 5A, 5B, and S13). Interestingly, a reduction in FoxP3-positive cells isolated from the spleens of VLP-treated mice was observed at the experimental endpoint (Figure 5C).

Next, we chose the LD + GM-CSF + OX40L VLPs to perform a second independent experiment to compare tumor inhibition in animals challenged with parental B16F10 tumor cells to animals challenged with PSMA-B16F10 cells. The animals were split into four experimental groups:the first two groups were challenged with B16F10 parental cells, and the other two groups were challenged with PSMA-B16F10 cells. These two main groups were then divided into two subgroups that were given LDCON VLPs (control VLP) and the targeted immunomodulatory LD + GM-CSF + OX40L VLP. It was observed that the mice challenged with PSMA-expressing tumors exhibited a substantial inhibition in tumor growth when treated with LD + GM-CSF + OX40L VLP and compared with mice challenged with parental B16F10 cells that lack the PSMA targeting ligand (Figure 6). The histological analysis of B16-PSMA tumors revealed an increased CD8 T cell infiltrate in the LD + GM-CSF + OX40L VLP-treated group, which corroborates the observed therapeutic effect (Figure S9).

DISCUSSION

In this work, we developed a new strategy for antitumor immunomodulation based on the use of VLPs derived from lentiviral capsids. These particles can express ligands to drive tropism to the tumor site and to confer immunomodulatory activity, besides driving soluble factors, as an anchored GM-CSF. Immunogenicity assays revealed a low humoral response to VLP antigens, which can be an advantage for systemic administration or even for multiple administration (Figure S10). This observation corroborates data from the literature demonstrating the great difficulty in developing robust humoral responses to HIV candidate vaccines.[61,62]

We recently demonstrated that EVs from antitumor vaccines harboring TNFSF 4-1BBL and OX40L have immunomodulatory

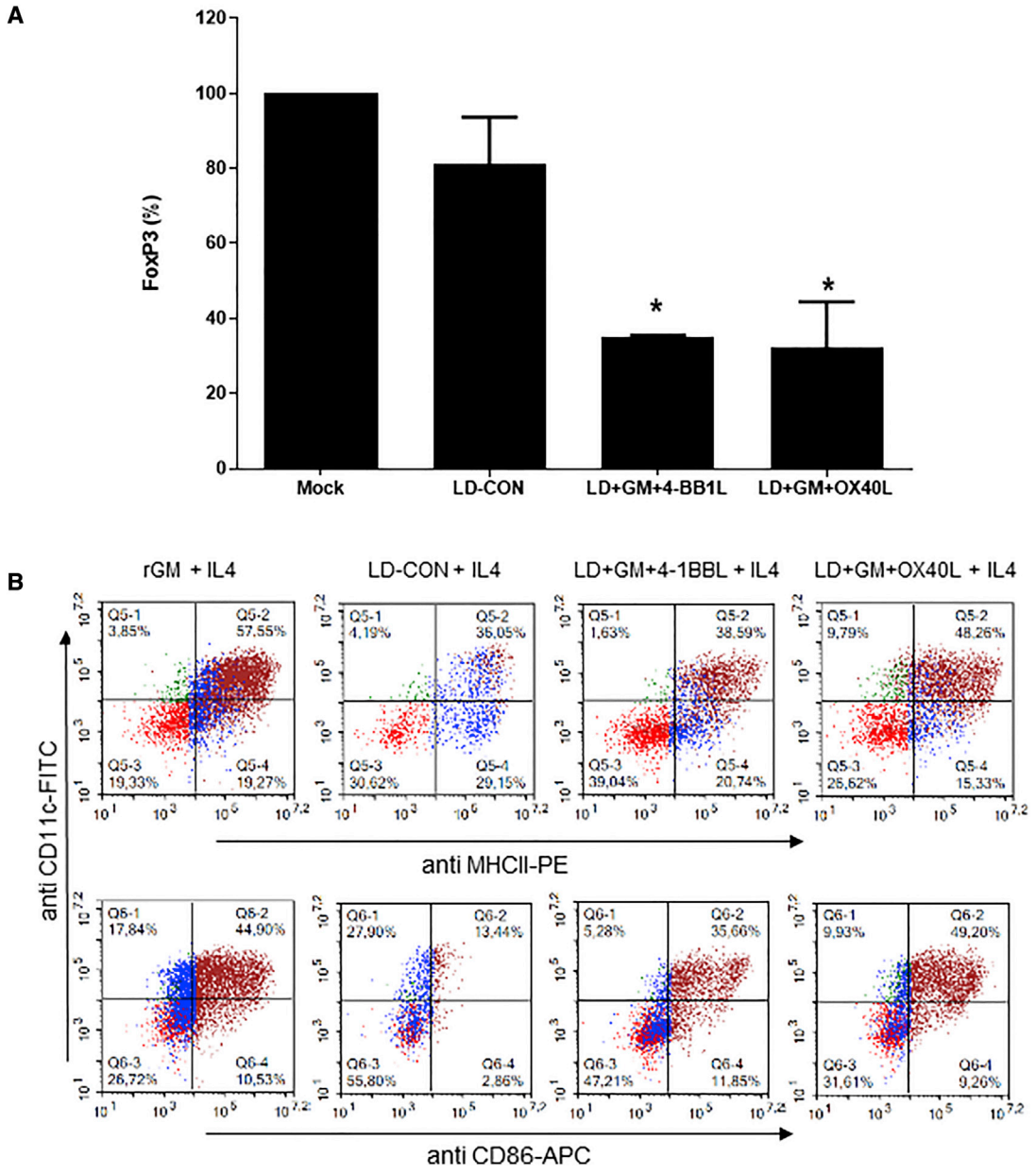

Figure 4. Functional characterization of trivalent LD-VLPs

(A) The trivalent VLPs harboring TNFSF ligands can inhibit the expression of FoxP3 transcription factor in regulatory T cells. The CD4 T cells that were isolated from the splenocytes of mice were induced *in vitro* for the regulatory T phenotype and then incubated with immunomodulatory VLPs (5×10^8 particles). The cells were stained with anti-FoxP3 APC to evaluate the expression of the FoxP3 transcription factor. Flow cytometry was performed and the data analyzed with the FCS Express 5 software. The graph shows the average percentage of FoxP3-positive cells and the respective error (SEM) of a representative experiment (N = 3). ANOVA and Dunnett tests were used in the statistical analysis considering significant values of $^*p < 0.05$ when compared with the LD-CON control. (B) VLPs harboring anchored GM-CSF induce typical markers of DC differentiation. Bone marrow cells were harvested from C57B/6 mice, and DC precursors (10^6 cells) were cultured with recombinant IL-4 (20 ng/mL), recombinant GM-CSF (20 ng/mL), or multivalent VLPs (5×10^9particles) that harbors GM-CSF. The cells were harvested after 7 days of incubation and labeled with anti-CD11c-FITC, anti-classII-MHC-PE, and anti-CD86-APC, performing flow cytometry. The graph represents 1 of 3 independent experiments. VLPs concentrations: LD-CON $1.76 \times 10^{13} \pm 1.06 \times 10^{12}$ particles/mL; LD + GM-CSF + 4-1BBL $1.12 \times 10^{13} \pm 1.58 \times 10^{12}$ particles/mL; LD + GM-CSF + OX40L $1.96 \times 10^{13} \pm 3.97 \times 10^{11}$ particles/mL.

activity, stimulating antitumor effects *in vitro*.[24] In contrast to EVs, in which a protocol for particle enrichment is required for labeling TNFSF ligands,[24] we observed that VLPs have greater versatility for expressing ligands on the particle surface and simplicity in preparation and labeling, which suggests higher efficiency in the process of generating the immunomodulatory particle derived from VLPs in

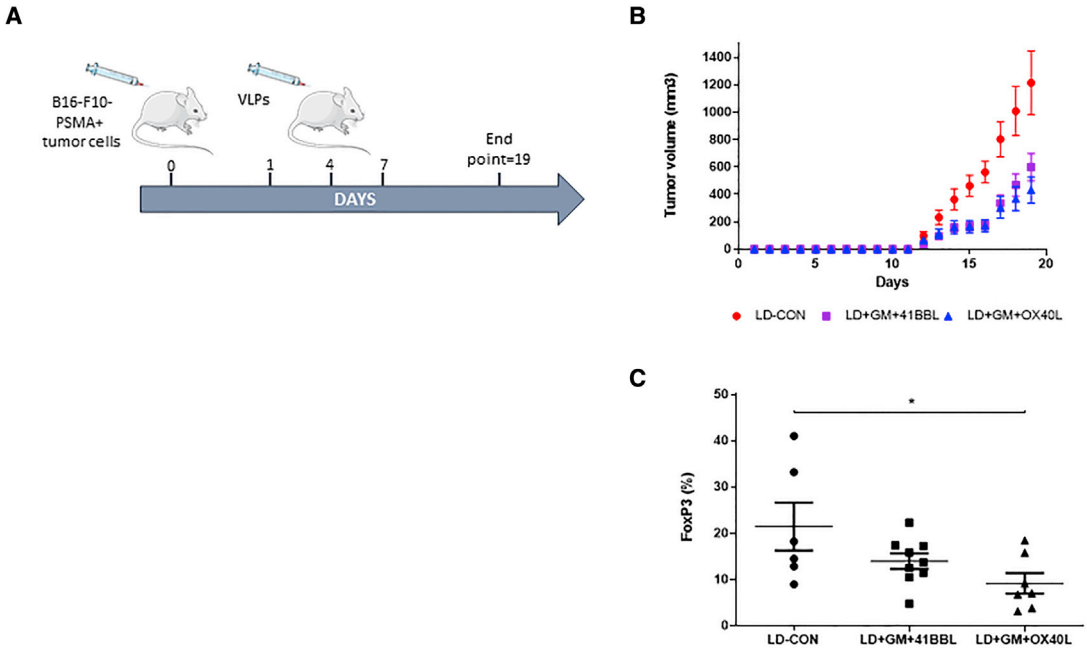

Figure 5. Immunomodulatory VLPs inhibit tumor growth in immunocompetent challenged mice

The immunocompetent C57/BL6 mice were challenged with syngeneic PSMA-expressing B16F10 cells and treated with the indicated VLPs. (A) Experimental design to compare the effect of LD + GM-CSF + 4-1BBL versus LD + GM-CSF + OX40L in animals challenged with B16F10-PSMA cells and (B) tumor growth curve. LDCON n = 8, LD + GM-CSF+ 4-1BBL n = 10, LD + GM + OX40L n = 7. Animals were injected subcutaneously with 10^5 B16F10-PSMA cells, as indicated in the experimental design. The VLPs were administrated as 2×10^{10} particles/100 μL, by intraperitoneal injection. The ANOVA and Dunnett tests were performed. (C) Animals were euthanized at the experimental endpoint and splenocytes were isolated and stained for FoxP3 following flow cytometry. LD-CON VLP (negative control, harbors only the PSMA LD ligand), LD + GM-CSF + 4-1BBL VLP (harbors LD ligand, anchored GM-CSF and 4-1BB ligand), LD + GM-CSF + OX40L VLP (harbors LD ligand, anchored GM-CSF, OX40L ligand). The tumor size for each animal is represented as mean and SEM, for each experimental group. The Student's t and Mann-Whitney *U* tests were performed (*$p < 0.05$). VLPs concentrations: LD-CON $1.76 \times 10^{13} \pm 1.06 \times 10^{12}$ particles/mL; LD + GM-CSF + 4-1BBL $1.12 \times 10^{13} \pm 1.58 \times 10^{12}$ particles/mL; LD + GM-CSF + OX40L $1.96 \times 10^{13} \pm 3.97 \times 10^{11}$ particles/mL.

comparison to EVs. The production protocol used in our experiments was based on centrifugation, which was enough for our proof of concept, but provided a low yield. The improvement in upstream processes, large-scale transfection protocols,[63,64] and downstream purification protocols, based on chromatography separation and tangential filtration,[65,66] will be essential to scaling up VLP for further applications. The lentiviral capsid-derived VLP platform demonstrated high plasticity, enabling the generation of VLPs with up to three different ligands. We have demonstrated that VLPs expressing the 4-1BB and OX40 ligands have *in vitro* functionality, increasing the production of IFN-gamma associated with Th1 cells and inducing the proliferation of these cells. Also, we found that VLPs that express the OX40 ligand reduce the conversion of FoxP3-positive cells and thereby inhibit the immunosuppression phenotype of Tregs. This phenomenon was consistent with the literature on the OX40 pathway.[17] In addition, we investigated the possibility of driving the tropism of the immunomodulatory particle to the tumor site using a targeting peptide anchored to the particle surface that specifically binds to the PSMA receptor.[50] The PSMA is a well-studied tumor antigen for imaging diagnostics and targeted radionuclide therapy of prostate cancer.[67] In addition to PSMA upregulation in prostate tumors, it has been reported to be expressed in tumor-associated vasculature of non-prostatic tumors such as breast cancer, bladder cancer, lung cancer, gastric cancer, colorectal cancer, brain cancer, and hepatocellular cancer, making it an attractive theranostic target.[43–49]

We generated multivalent VLPs harboring immunomodulatory molecules and a PSMA-driving ligand. In fact, we confirmed the PSMA-specific targeting by confocal microscopy. We observed that targeting the VLP with the PSMA ligand induced the elimination of tumors in animals challenged with syngeneic tumor cells expressing PSMA. Our delivery system also allows us to drive soluble proteins such as GM-CSF, which was anchored to the surface of the particle. In this way, GM-CSF could be directly driven to the tumor site, where the immunomodulator may potentiate the differentiation of dendritic cells.[68] Targeting the delivery of GM-CSF may enhance its concentration at the tumor site and may also contribute to reducing the possibility of the unwanted effects associated with an eventual GM-CSF systemic distribution.[69] It is interesting to note that the same strategy used to anchor GM-CSF on the surface of the VLP could also be used for other soluble molecules. In our experiments, we have observed that targeting VLPs showed therapeutic benefits in challenged animals. In this way, we have demonstrated the possibility of engineering multifunctional VLPs for the targeted delivery of immunomodulators. These particles inhibited tumor growth in challenged animals, opening new perspectives for the development of alternative antitumor approaches.

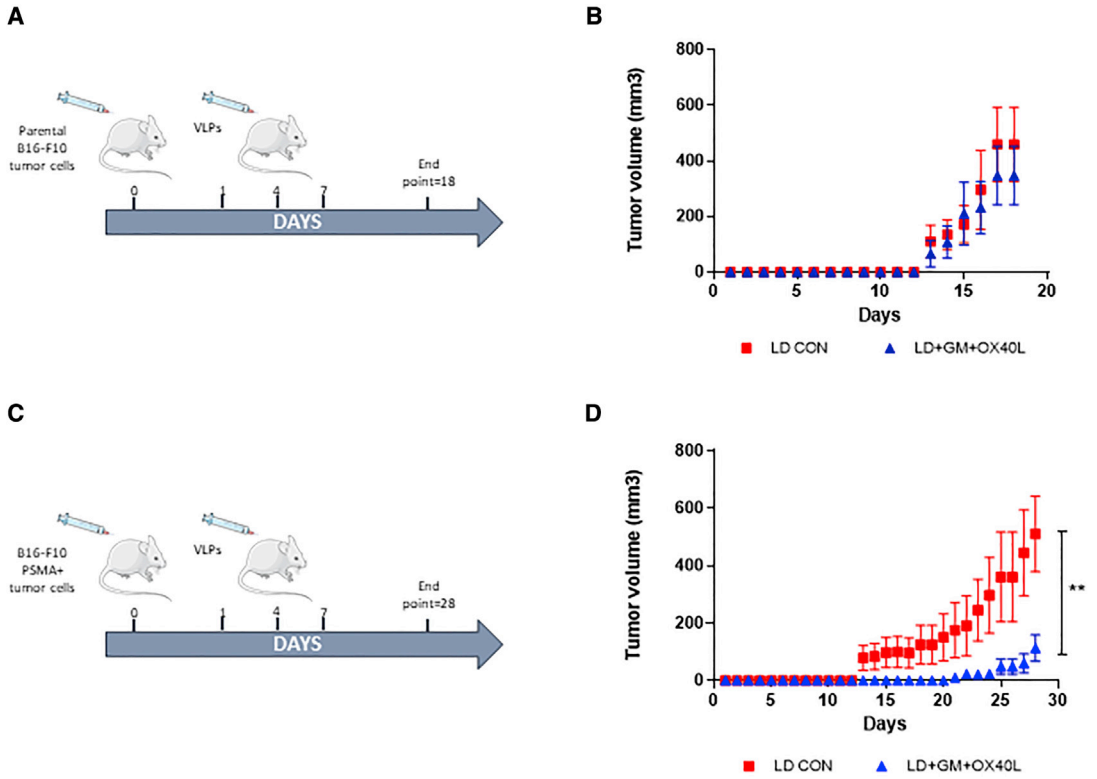

Figure 6. PSMA-targeted immunomodulatory VLPs inhibit tumor growth in PSMA-B16F10 challenged animals

(A) Experimental design to compare the effect of LD + GM-CSF + OX40L versus LD CON in animals challenged with parental B16F10 cells and (B) tumor growth curve. N = 5 animals per group. (C) Experimental design to compare the effect of LD + GM-CSF + OX40L versus LD-CON in animals challenged with B16F10-PSMA cells and (D) tumor growth curve. n= 5 animals per group. Animals were injected subcutaneously with 5×10^4 of parental B16F10 cells or 10^5 B16F10-PSMA cells as indicated in the experimental design. Each animal was given 2×10^{10} of indicated VLPs in 100 μL by intraperitoneal injection. The tumor size of each animal was represented as mean and SEM for each experimental group. The Student's t and Mann-Whitney *U* tests were performed (**$p < 0.05$). VLP concentrations; LD-CON $2.52 \times 10^{11} \pm 9.63 \times 10^9$ particles/mL; LD + GM-CSF + OX40L 5.77×10^{11} +/− 2.22×10^{10} particles/mL).

MATERIALS AND METHODS

Generation of plasmids, viral vectors, and cell lines

The cDNA of 4-1BBL, OX40L, and GM-CSF were PCR amplified from mice splenocytes and cloned into linearized pCDNA3.1-hygro + vector (Invitrogen, USA). A cassette encoding the cDNA for the PSMA LD ligand was synthetized based on a previously described DNA sequence[50] and cloned into a CMV driven expression vector (pDP), in frame to a 5′ IgK signal peptide and a 3′ platelet-derived growth factor (PDGF) transmembrane portion. The 3T3-4-1BB cell pool was established by transducing NIH3T3 cells with the pCL-4-1BB retrovirus, which encodes CD137 and G418 resistance[19] (Figure S11A). The B16F10-PSMA cell pool was established via the retroviral transduction of B16F10 with SFG-PSMA, which encodes the PSMA gene and resistance to puromycin (Figure S11B). Viral vectors were generated with amphotropic plasmids and titrated by the Viral Vector Facility at LNBio. Oligo sequences are listed in Figure S12.

Production of immunomodulatory VLPs

The VLPs were produced by the transient transfection of HEK293T cells with a psPAX2 plasmid that encodes the VLP capsid and additional pCDNA3.1-derived plasmids the encode the VLP surface ligands. Transfected cells were cultivated in Dulbecco's Modified Eagle's Medium (DMEM) supplemented with 1% penicillin/streptomycin, 1% glutamine, and 10% fetal bovine serum (FBS). Control VLPs were produced by co-transfecting the pCDNA3.1-Hygro + vector and psPAX2 (pSPAXplasmid: 15μg + pCDNA plasmid: 6 μg for each ligand vector). To assess transfection efficiency, VLP-producing cells were stained with anti-4-1BBL PE (eBioscience clone TKS, eBioscience, Hatfield, UK), anti-OX40L PE (eBioscience clone OX89), and anti-GM-CSF PE (eBioscience clone MP1 -22 $\times$ 10^9) following flow cytometry (Figure S1). VLP preparations were concentrated by ultracentrifugation at 100,000 $\times$ *g* for 1.5 h and resuspended in 1$\times$ PBS and stored at −80°C.

Quantification of VLPs by nanoparticle tracking analysis

The concentration of VLPs was estimated by nanoparticle tracking analysis (NTA). The preparations of VLPs were diluted in 1$\times$ PBS to reach a concentration between 10^8 and 10^9 particles/mL and read into the NanoSight NS300 instrument. It acquired 3 videos of 30 s per sample, at 18°C. Both particle size and concentration were

defined as an average of measures of analyzed videos using the NTA 3.1 software (Malvern Instruments, Worcestershire, UK).

Phenotypic characterization of VLPs by flow cytometry

To verify the presence of the OX40L, 4-1BBL, and anchored GM-CSF and LD ligands on the surface of the VLPs, we performed flow cytometry of VLPs bound to micrometric polystyrene particles (Polybead microspheres, Polysciences, Warrington, PA, USA). For the detection of OX40L and 4-1BBL, 5×10^4 beads were previously loaded with 1 μg capture anti-4-1BBL antibodies (eBioscience clone TKS-1) or anti-OX40L (eBioscience clone OX89) and incubated to 10^9 4-1BBL + OX40L bivalent VLPs or CON VLPs. These beads with antibodies and VLPs were stained with anti-4-1BBL PE or anti-OX40L PE and flow cytometry was performed. To verify the LD ligand, beads were previously loaded with the PSMA protein. Briefly, 5×10^4 beads were incubated with anti-PSMA antibody (clone LNI-17, BioLegend, San Diego, CA, USA) and then incubated with a lysate of PSMA-expressing NIH-3T3 cells (Figure S10C). The VLPs LD + GM-CSF + 4-1BBL, LD + GM-CSF + OX40L and LD-CON VLPs were added to the PSMA beads labeled with anti-4-1BBL PE, anti-OX40L PE, and anti-GM-CSF PE antibodies following flow cytometry.

Transmission electron microscopy (TEM)

Negative-staining electron microscopy of VLPs was adapted from Semionatto et al.[24] The 4-1BBL + OX40L VLPs were fixed in 2% uranyl acetates and transferred to 400-mesh copper grids coated by an ultra-thin carbon film superimposed on a Lacey carbon film (Ted Pella, Redding, CA, USA). Images were acquired through a transmission electron microscope (PELCO easiGlow, Ted Pella) equipped with tungsten filament and operated at 120 kV and analyzed using Gatan Digital Micrograph (GMS3) software and ImageJ Fiji software (ImageJ, National Institutes of Health, Rockville, MD, USA).

Confocal microscopy

B16F10 or B16F10-PSMA-positive cells were seeded into glass-bottom microwell dishes (3×10^5 cells/well) and incubated with LD + GM-CSF + 4-1BBL VLPs, to a final concentration of 3×10^{10} particles/mL. The cells were stained with a biotin anti-41BBL (BioLegend clone TKS-1) and incubated for 1 h with streptavidin Alexa Fluor 647 (BioLegend) at concentrations of 1:100 and 2:500, respectively. Images were acquired on a Leica TCS SP8 confocal microscope with 63×/100× objective lenses and processed with ImageJ software.

Purification of primary CD4 T cells and antigen-presenting cells (APCs)

Isolation of primary CD4 T cells was performed with murine spleen cells by using a murine CD4 T cell isolation kit (EasySep mouse $CD4^+$ T cell isolation kit) according to the manufacturer's instructions. The purity of the resulting T cell populations was confirmed to be higher than 95% by flow cytometry (data not shown). The APCs were purified from murine splenocytes and treated with mitomycin C. All of the cells were cultured in complete medium (10% FBS RPMI, 1% penicillin/streptomycin, 1× glutamine, 1% HEPES, 1% sodium pyruvate, 1% non-essential amino acids, and 50μM β-mercaptoethanol) supplemented with IL-2 (50 U/mL). The cells were incubated at 37°C in 5% CO_2.

In vitro T cell proliferation and ELISA assay

In this assay, 5×10^4 CD4 T cells isolated from the splenocytes of C57BL/6 mice were stained with CFSE and cultivated in the presence of 0.5 μg/mL anti-CD3 antibody (eBioscience clone 17A2) and 5×10^4 APC cells in 96-well plates, with supplemented RPMI medium as previously described. The experimental groups were prepared in 4 replicates, adding 2×10^8 VLP particles for each well. For the mock control, VLPs were not added, but CD4 T cells, APCs, and anti-CD3 antibody were added. The cells were cultivated for 72 h at 37°C and 5% CO_2. After that period, the cells were harvested and resuspended in 1× PBS to perform flow cytometry. The proliferation of CD4 T cells was evaluated as a function of the CFSE fluorescence intensity decay (fluorescein isothiocyanate [FITC]) and the data were analyzed using the FCS Express 5 flow cytometry software (De Novo Software, Pasadena, CA, USA).

The IFN-gamma concentration was determined by ELISA, using the pooled supernatant of replicates for each experimental group. The ELISA assay was performed in triplicate using the mouse IFN-gamma Quantikine ELISA kit (R&D Systems, Minneapolis, MN, USA) per the manufacturer's instructions.

Generation of inducible regulatory T cells

To generate iTRs, 2×10^5 CD4 T cells previously isolated from C57BL/6 mice spleens were pre-activated in a 24-well plate with 1 μg/mL anti-CD3 (eBioscience clone 17A2) and anti-CD28 antibodies (eBioscience clone 37.51), with RPMI medium supplemented with 50 U/mL IL-2. The activated CD4 T cells were cultivated for 24 h at 37°C in 5% CO_2 and were given an iTR induction cocktail containing IL-2 (100 U/mL, PeproTech, Cranbury, NJ, USA), TGF-β (1 ng/mL PeproTech), and retinoic acid (100 nM). VLPs were added to the indicated wells. The cells were cultivated for 48 h at 37°C in 5% CO_2, harvested and permeabilized using the Foxp3 transcription factor staining buffer set (eBioscience) following the manufacturer's instructions, and then stained with the anti-FoxP3 antibody APC (eBioscience clone FJK-16s) or the control isotype (eBioscience rat/IgG2a immunoglobulin G2a], APC kappa). Flow cytometry was performed to measure FoxP3 expression, and the data were analyzed using the FCS Express 5 flow cytometry software.

In vitro Treg suppression assays

In this protocol, Tconv were stained with CFSE and cultivated with iTR, using a ratio of 1:8 (Treg:Tconv), in the presence of 0.5 μg/mL anti-CD3 stimuli (eBioscience clone 17A2). The cells were cultivated 72 h following flow cytometry. The immunosuppression capacity of iTR cells was determined based on the inhibition of conventional T cell proliferation and was evaluated as a function of the CFSE fluorescence intensity decay (FITC). The data were analyzed using the FCS Express 5 flow cytometry software.

In vitro *assay to evaluate the induction of antitumor response mediated by immune cells*

In this assay, B16-F10 tumor cells expressing the GFP reporter were incubated with splenocytes and VLPs preparations. The rationale of this experiment was that the VLPs preparation could co-stimulate T cells, potentiating the elimination of B16-F10 GFP-positive cells. Briefly, 1,000 B16-F10 GFP cells per well were seeded in 96-well plates, adding the same numbers of C57BL/6 splenocytes and 2×10^8 VLPs. After 72 h of incubation, the splenocytes were removed and the adherent tumor cells were fixed with 4% paraformaldehyde (PFA) and stained with DAPI (Sigma). The quantification was performed by the Operetta HTS Imaging System (PerkinElmer). Each well was evaluated in 75 different fields using 20× magnification. All of the images were analyzed using Columbus software, version 2.4.0 (PerkinElmer), and representative images were processed with the bio-formats plugin in FIJI.

Generation of bone marrow-derived DCs (BMDCs)

BMDCs were obtained by washing the tibiae and femurs of mice with cold PBS and separating cells using a 70-μm cell strainer. The cells were seeded in a 24-well plate (10^6 cells/well) with conditioned medium (RPMI with 1% penicillin/streptomycin, 10% FBS, glutamine, 1% HEPES, 1% sodium pyruvate, 1% non-essential amino acids, and 50μM β-mercaptoethanol) supplemented with GM-CSF (20 ng/mL, R&D Systems), or GM-CSF VLPs (LD + GM-CSF + 4-1BBL or LD + GM-CSF + OX40L, 5×10^9 particle/mL), and IL-4 (20 ng/mL, R&D Systems). The cells were characterized by flow cytometry labeling surface markers CD11c (FITC anti-mouse CD11c, BioLegend), MHC class II (PE anti-mouse MHC II, BioLegend) and CD86 (APC anti-mouse CD86, BioLegend). The data were analyzed using the ACEA NovoCyte 2000 flow cytometer.

In vivo experiments

C57BL/6 mice were given subcutaneous injections of 5×10^4 B16F10 or B16F10-PSMA tumor cells in the left flank on day 0 of the experiment and split into experimental groups. On days 1, 4, and 7, each group was intraperitoneally administrated with the indicated VLPs or 1× PBS. The animals were monitored daily, quantifying the tumor volume with a caliper. The tumor volume was calculated based on three perpendicular measurements. The animals were sacrificed between days 20 and 28, depending on the development of the tumors from the control groups. The mice exhibiting any sign of behavior alteration that could indicate stress or suffering were sacrificed before the endpoint and removed from the experiment. The protocol was approved by the ethics animal committee from the National Center for Research in Energy and Materials (CNPEM) (protocol CEUA-35/2018).

VLP immunogenicity assay

C57BL/6 mice were randomly divided into 4 groups (N = 4: PBS, VLP, Freund's adjuvant, VLP + Freund's adjuvant and severe acute respiratory syndrome-coronavirus-2 (SARS-CoV-2) + Freund's adjuvant. The animals were immunized on days 0, 14, and 28 with a dose of 100 μL via intraperitoneal injection. The dose of VLP was 4×10^{10} particles per injection, the SARS-CoV-2 virus was 10^5 particles per injection, and Freund's adjuvant (Sigma-Aldrich) was mixed in a v/v ratio. After 35 days, the animals were sacrificed and blood was collected via the retro-orbital plexus to determine the immunity-related indices. IgG titers in the sera were measured by sandwich ELISA. Briefly, precoated plates with goat anti-mouse IgG (1 μg/mL, Thermo Fisher) were incubated with the samples of the sera of the experimental groups at a dilution of 1:500. After washing, the total IgG titer was detected with rabbit anti-mouse IgG antibody, Fc, horseradish peroxidase (HRP) conjugate (Thermo Fisher) in a 1:10,000 dilution, using 3,3′,5,5′-tetramethylbenzidine TMB (Thermo Fisher) as a chromogen substrate.

Immunohistochemistry of tumors

Immunohistochemistry was performed using 5-μm-thick sections of tumor tissue fixed in 4% PFA and embedded in paraffin. Sections were deparaffinized and hydrated using xylol and ethanol followed by antigen unmasking using 1× citrate unmasking solution (cat. no. 14746, Cell Signaling Technology, Danvers, MA, USA) for 10 min at 95°C. Subsequently, tissues were treated with 3% hydrogen peroxide for 10 min and then were washed with 1× Tris-buffered saline with Tween 20 (TBST) (Cell Signaling Technology, cat. no. 9997) followed by blocking with 100 μL TBST/5% normal goat serum (Cell Signaling Technology, cat. no. 5425) for 1 h at room temperature. The blocking solution was removed and 100 μL of primary antibody CD8α (D4W2Z) XP Rabbit monoclonal antibody (mAb) (Cell Signaling Technology, cat. no. 98941) diluted 1:200 in SignalStain antibody diluent (Cell Signaling Technology, cat. no. 8112) was added to each section and incubated overnight at 4°C. They were washed with the wash buffer 3 times for 5 min each and covered with drops of SignalStain Boost detection reagent (HRP, rabbit) (Cell Signaling Technology, cat. no. #8114) and incubated in a humidified chamber for 30 min at room temperature. Sections were washed three times with wash buffer and 100μL SignalStain DAB (Cell Signaling, cat #8059) were added to each section. The slides were dipped in dH2O and counterstained with hematoxylin and then mounted using SignalStain Mounting Medium (Cell Signaling Technology, cat. no. 14177). Images were captured using a Leica confocal microscope and images were analyzed using LAS AF software (Leica, Wetzlar, Germany).

Statistical analysis

The statistical analysis of the data was performed using GraphPad Prism version 5.00 (GraphPad, San Diego, CA, USA). One-way ANOVA followed by the Dunnett's test was used in experiments with more than three experimental groups. The Student's t test and the Mann-Whitney *U* test was applied to analyze data from *in vivo* experiments, comparing the effect of the therapeutic and control VLPs. The data were represented as the mean and the standard error of the mean (SEM), and $p \leq 0.05$ was considered statistically significant.

SUPPLEMENTAL INFORMATION

Supplemental information can be found online at https://doi.org/10.1016/j.omto.2022.02.010.

ACKNOWLEDGMENTS

We thank Eugenia Camargo for technical support in cloning and flow cytometry, LVV-LNBio for viral preparations, LOM-LNBio for support with the animal experiments, LIB-LNBio for confocal microscopy support, and TEM-LNNano for TEM support. We thank Fundação de Amparo à Pesquisa do Estado de São Paulo (FAPESP) for financial support grants 2015/01488-2 and 2019/04458-8 (to M.C.B.). We also thank Coordenação de Aperfeiçoamento de Pessoal de Nível Superior (CAPES) for PhD fellowship to S.P.

AUTHOR CONTRIBUTIONS

S.P. planned and performed the experiments, analyzed the data, and wrote the manuscript. J.M.T., I.F.S., L.P.R., R.S.M.R., A.J.M.-R., and M.C.F. performed the experiments and analyzed the data. P.S.L.O. discussed strategies and results. M.C.B. supervised the study, planned the experiments, analyzed the data, provided the funding, and wrote the manuscript. All of the authors contributed to the article and approved the submitted version.

DECLARATION OF INTERESTS

The authors declare no competing interests.

REFERENCES

1. Perez-Ruiz, E., Melero, I., Kopecka, J., Sarmento-Ribeiro, A.B., Garcia-Aranda, M., and De Las Rivas, J. (2020). Cancer immunotherapy resistance based on immune checkpoints inhibitors: targets, biomarkers, and remedies. Drug Resist. Updat. *53*, 100718. https://doi.org/10.1016/j.drup.2020.100718.

2. Jackson, C.M., Choi, J., and Lim, M. (2019). Mechanisms of immunotherapy resistance: lessons from glioblastoma. Nat. Immunol. *20*, 1100–1109. https://doi.org/10.1038/s41590-019-0433-y.

3. Darvin, P., Toor, S.M., Sasidharan Nair, V., and Elkord, E. (2018). Immune checkpoint inhibitors: recent progress and potential biomarkers. Exp. Mol. Med. *50*, 165. https://doi.org/10.1038/s12276-018-0191-1.

4. Pardoll, D.M. (2012). The blockade of immune checkpoints in cancer immunotherapy. Nat. Rev. Cancer *12*, 252–264. https://doi.org/10.1038/nrc3239.

5. Robert, C. (2020). A decade of immune-checkpoint inhibitors in cancer therapy. Nat. Commun. *11*, 3801. https://doi.org/10.1038/s41467-020-17670-y.

6. He, X., and Xu, C. (2020). Immune checkpoint signaling and cancer immunotherapy. Cell Res. *30*, 660–669. https://doi.org/10.1038/s41422-020-0343-4.

7. Moran, A.E., Kovacsovics-Bankowski, M., and Weinberg, A.D. (2013). The TNFRs OX40, 4-1BB, and CD40 as targets for cancer immunotherapy. Curr. Opin. Immunol. *25*, 230–237. https://doi.org/10.1016/j.coi.2013.01.004.

8. Mascarelli, D.E., Rosa, R.S.M., Toscaro, J.M., Semionatto, I.F., Ruas, L.P., Fogagnolo, C.T., Lima, G.C., and Bajgelman, M.C. (2021). Boosting antitumor response by costimulatory strategies driven to 4-1BB and OX40 T-cell receptors. Front Cell Dev. Biol. *9*, 692982. https://doi.org/10.3389/fcell.2021.692982.

9. Croft, M., So, T., Duan, W., and Soroosh, P. (2009). The significance of OX40 and OX40L to T-cell biology and immune disease. Immunol. Rev. *229*, 173–191. https://doi.org/10.1111/j.1600-065X.2009.00766.x.

10. Melero, I., Shuford, W.W., Newby, S.A., Aruffo, A., Ledbetter, J.A., Hellstrom, K.E., Mittler, R.S., and Chen, L. (1997). Monoclonal antibodies against the 4-1BB T-cell activation molecule eradicate established tumors. Nat. Med. *3*, 682–685.

11. Houot, R., Goldstein, M.J., Kohrt, H.E., Myklebust, J.H., Alizadeh, A.A., Lin, J.T., Irish, J.M., Torchia, J.A., Kolstad, A., Chen, L., and Levy, R. (2009). Therapeutic effect of CD137 immunomodulation in lymphoma and its enhancement by Treg depletion. Blood *114*, 3431–3438. https://doi.org/10.1182/blood-2009-05-223958.

12. Gauttier, V., Judor, J.P., Le Guen, V., Cany, J., Ferry, N., and Conchon, S. (2014). Agonistic anti-CD137 antibody treatment leads to antitumor response in mice with liver cancer. Int. J. Cancer *135*, 2857–2867. https://doi.org/10.1002/ijc.28943.

13. Sznol, M., Hodi, F.S., Margolin, K., McDermott, D.F., Ernstoff, M.S., Kirkwood, J.M., Wojtaszek, C., Feltquate, D., and Logan, T. (2008). Phase I study of BMS-663513, a fully human anti-CD137 agonist monoclonal antibody, in patients (pts) with advanced cancer (CA). J. Clin. Oncol. *26*, 3007.

14. Petty, J.K., He, K., Corless, C.L., Vetto, J.T., and Weinberg, A.D. (2002). Survival in human colorectal cancer correlates with expression of the T-cell costimulatory molecule OX-40 (CD134). Am. J. Surg. *183*, 512–518.

15. Ladanyi, A., Somlai, B., Gilde, K., Fejos, Z., Gaudi, I., and Timar, J. (2004). T-cell activation marker expression on tumor-infiltrating lymphocytes as prognostic factor in cutaneous malignant melanoma. Clin. Cancer Res. *10*, 521–530.

16. Piconese, S., Valzasina, B., and Colombo, M.P. (2008). OX40 triggering blocks suppression by regulatory T cells and facilitates tumor rejection. J. Exp. Med. *205*, 825–839. https://doi.org/10.1084/jem.20071341.

17. So, T., and Croft, M. (2007). Cutting edge: OX40 inhibits TGF-beta- and antigen-driven conversion of naive CD4 T cells into CD25+Foxp3+ T cells. J. Immunol. *179*, 1427–1430.

18. Innamarato, P., Asby, S., Morse, J., Mackay, A., Hall, M., Kidd, S., Nagle, L., Sarnaik, A.A., and Pilon-Thomas, S. (2020). Intratumoral activation of 41BB costimulatory signals enhances CD8 T cell expansion and modulates tumor-infiltrating myeloid cells. J. Immunol. *205*, 2893–2904. https://doi.org/10.4049/jimmunol.2000759.

19. Manrique-Rincon, A.J., Beraldo, C.M., Toscaro, J.M., and Bajgelman, M.C. (2017). Exploring synergy in combinations of tumor-derived vaccines that harbor 4-1BBL, OX40L, and GM-CSF. Front. Immunol. *8*, 1150. https://doi.org/10.3389/fimmu.2017.01150.

20. Gramaglia, I., Weinberg, A.D., Lemon, M., and Croft, M. (1998). Ox-40 ligand: a potent costimulatory molecule for sustaining primary CD4 T cell responses. J. Immunol. *161*, 6510–6517.

21. Adappa, N.D., Sung, C.K., Choi, B., Huang, T.G., Genden, E.M., and Shin, E.J. (2008). The administration of IL-12/GM-CSF and Ig-4-1BB ligand markedly decreases murine floor of mouth squamous cell cancer. Otolaryngol. Head Neck Surg. *139*, 442–448. https://doi.org/10.1016/j.otohns.2008.05.001.

22. McNamara, J.O., Kolonias, D., Pastor, F., Mittler, R.S., Chen, L., Giangrande, P.H., Sullenger, B., and Gilboa, E. (2008). Multivalent 4-1BB binding aptamers costimulate CD8+ T cells and inhibit tumor growth in mice. J. Clin. Invest. *118*, 376–386. https://doi.org/10.1172/JCI33365.

23. Dollins, C.M., Nair, S., Boczkowski, D., Lee, J., Layzer, J.M., Gilboa, E., and Sullenger, B.A. (2008). Assembling OX40 aptamers on a molecular scaffold to create a receptor-activating aptamer. Chem. Biol. *15*, 675–682. https://doi.org/10.1016/j.chembiol.2008.05.016.

24. Semionatto, I.F., Palameta, S., Toscaro, J.M., Manrique-Rincón, A.J., Ruas, L.P., Paes Leme, A.F., and Bajgelman, M.C. (2020). Extracellular vesicles produced by immunomodulatory cells harboring OX40 ligand and 4-1BB ligand enhance antitumor immunity. Sci. Rep. *10*, 15160. https://doi.org/10.1038/s41598-020-72122-3.

25. van Niel, G., D'Angelo, G., and Raposo, G. (2018). Shedding light on the cell biology of extracellular vesicles. Na. Rev. Mol. Cell Biol. *19*, 213–228. https://doi.org/10.1038/nrm.2017.125.

26. Gould, S.J., Booth, A.M., and Hildreth, J.E. (2003). The Trojan exosome hypothesis. Proc. Natl. Acad. Sci. U S A. *100*, 10592–10597. https://doi.org/10.1073/pnas.1831413100.

27. Venereo-Sanchez, A., Fulton, K., Koczka, K., Twine, S., Chahal, P., Ansorge, S., Gilbert, R., Henry, O., and Kamen, A. (2019). Characterization of influenza H1N1 Gag virus-like particles and extracellular vesicles co-produced in HEK-293SF. Vaccine *37*, 7100–7107. https://doi.org/10.1016/j.vaccine.2019.07.057.

28. Li, K., Peers-Adams, A., Win, S.J., Scullion, S., Wilson, M., Young, V.L., Jennings, P., Ward, V.K., Baird, M.A., and Young, S.L. (2013). Antigen incorporated in virus-like particles is delivered to specific dendritic cell subsets that induce an effective antitumor immune response in vivo. J. Immunother. *36*, 11–19. https://doi.org/10.1097/CJI.0b013e3182787f5e.

29. Nooraei, S., Bahrulolum, H., Hoseini, Z.S., Katalani, C., Hajizade, A., Easton, A.J., and Ahmadian, G. (2021). Virus-like particles: preparation, immunogenicity and their

roles as nanovaccines and drug nanocarriers. J. Nanobiotechnol. *19*, 59. https://doi.org/10.1186/s12951-021-00806-7.

30. Caldeira, J.C., Perrine, M., Pericle, F., and Cavallo, F. (2020). Virus-like particles as an immunogenic platform for cancer vaccines. Viruses *12*. https://doi.org/10.3390/v12050488.

31. Chen, C.C., Xing, L., Stark, M., Ou, T., Holla, P., Xiao, K., Kamita, S.G., Hammock, B.D., Lam, K., and Cheng, R.H. (2016). Chemically activatable viral capsid functionalized for cancer targeting. Nanomedicine (Lond) *11*, 377–390. https://doi.org/10.2217/nnm.15.207.

32. Kim, H., Choi, H., Bae, Y., and Kang, S. (2019). Development of target-tunable P22 VLP-based delivery nanoplatforms using bacterial superglue. Biotechnol. Bioeng. *116*, 2843–2851. https://doi.org/10.1002/bit.27129.

33. Ghosh, S., and Banerjee, M. (2021). A smart viral vector for targeted delivery of hydrophobic drugs. Sci. Rep. *11*, 7030. https://doi.org/10.1038/s41598-021-86198-y.

34. Bolli, E., O'Rourke, J.P., Conti, L., Lanzardo, S., Rolih, V., Christen, J.M., Barutello, G., Forni, M., Pericle, F., and Cavallo, F. (2018). A Virus-Like-Particle immunotherapy targeting Epitope-Specific anti-xCT expressed on cancer stem cell inhibits the progression of metastatic cancer in vivo. Oncoimmunology *7*, e1408746. https://doi.org/10.1080/2162402X.2017.1408746.

35. Cubas, R., Zhang, S., Li, M., Chen, C., and Yao, Q. (2011). Chimeric Trop2 virus-like particles: a potential immunotherapeutic approach against pancreatic cancer. J. Immunother. *34*, 251–263. https://doi.org/10.1097/CJI.0b013e318209ee72.

36. Lizotte, P.H., Wen, A.M., Sheen, M.R., Fields, J., Rojanasopondist, P., Steinmetz, N.F., and Fiering, S. (2016). In situ vaccination with cowpea mosaic virus nanoparticles suppresses metastatic cancer. Nat. Nanotechnol. *11*, 295–303. https://doi.org/10.1038/nnano.2015.292.

37. Palladini, A., Thrane, S., Janitzek, C.M., Pihl, J., Clemmensen, S.B., de Jongh, W.A., Clausen, T.M., Nicoletti, G., Landuzzi, L., Penichet, M.L., et al. (2018). Virus-like particle display of HER2 induces potent anti-cancer responses. Oncoimmunology *7*, e1408749. https://doi.org/10.1080/2162402X.2017.1408749.

38. Tumban, E., Muttil, P., Escobar, C.A., Peabody, J., Wafula, D., Peabody, D.S., and Chackerian, B. (2015). Preclinical refinements of a broadly protective VLP-based HPV vaccine targeting the minor capsid protein, L2. Vaccine *33*, 3346–3353. https://doi.org/10.1016/j.vaccine.2015.05.016.

39. Naldini, L., Blomer, U., Gage, F.H., Trono, D., and Verma, I.M. (1996). Efficient transfer, integration, and sustained long-term expression of the transgene in adult rat brains injected with a lentiviral vector. Proc. Natl. Acad. Sci. U S A. *93*, 11382–11388.

40. Zufferey, R., Nagy, D., Mandel, R.J., Naldini, L., and Trono, D. (1997). Multiply attenuated lentiviral vector achieves efficient gene delivery in vivo. Nat. Biotechnol. *15*, 871–875. https://doi.org/10.1038/nbt0997-871.

41. Page, K.A., Landau, N.R., and Littman, D.R. (1990). Construction and use of a human immunodeficiency virus vector for analysis of virus infectivity. J. Virol. *64*, 5270–5276. https://doi.org/10.1128/JVI.64.11.5270-5276.1990.

42. Watson, D.J., Kobinger, G.P., Passini, M.A., Wilson, J.M., and Wolfe, J.H. (2002). Targeted transduction patterns in the mouse brain by lentivirus vectors pseudotyped with VSV, Ebola, Mokola, LCMV, or MuLV envelope proteins. Mol. Ther. *5*, 528–537. https://doi.org/10.1006/mthe.2002.0584.

43. Chang, S.S., Reuter, V.E., Heston, W.D., Bander, N.H., Grauer, L.S., and Gaudin, P.B. (1999). Five different anti-prostate-specific membrane antigen (PSMA) antibodies confirm PSMA expression in tumor-associated neovasculature. Cancer Res. *59*, 3192–3198.

44. Haffner, M.C., Kronberger, I.E., Ross, J.S., Sheehan, C.E., Zitt, M., Muhlmann, G., Ofner, D., Zelger, B., Ensinger, C., Yang, X.J., et al. (2009). Prostate-specific membrane antigen expression in the neovasculature of gastric and colorectal cancers. Hum. Pathol. *40*, 1754–1761. https://doi.org/10.1016/j.humpath.2009.06.003.

45. Holzgreve, A., Biczok, A., Ruf, V.C., Liesche-Starnecker, F., Steiger, K., Kirchner, M.A., Unterrainer, M., Mittlmeier, L., Herms, J., Schlegel, J., et al. (2021). PSMA expression in glioblastoma as a basis for theranostic approaches: a retrospective, correlational panel study including immunohistochemistry, clinical parameters and PET imaging. Front. Oncol. *11*, 646387. https://doi.org/10.3389/fonc.2021.646387.

46. Jiao, D., Li, Y., Yang, F., Han, D., Wu, J., Shi, S., Tian, F., Guo, Z., Xi, W., Li, G., et al. (2019). Expression of prostate-specific membrane antigen in tumor-associated vasculature predicts poor prognosis in hepatocellular carcinoma. Clin. Transl Gastroenterol. *10*, 1–7. https://doi.org/10.14309/ctg.0000000000000041.

47. Samplaski, M.K., Heston, W., Elson, P., Magi-Galluzzi, C., and Hansel, D.E. (2011). Folate hydrolase (prostate-specific membrane [corrected] antigen) 1 expression in bladder cancer subtypes and associated tumor neovasculature. Mod. Pathol. *24*, 1521–1529. https://doi.org/10.1038/modpathol.2011.112.

48. Wang, H.L., Wang, S.S., Song, W.H., Pan, Y., Yu, H.P., Si, T.G., Liu, Y., Cui, X.N., and Guo, Z. (2015). Expression of prostate-specific membrane antigen in lung cancer cells and tumor neovasculature endothelial cells and its clinical significance. PLoS One *10*, e0125924. https://doi.org/10.1371/journal.pone.0125924.

49. Wernicke, A.G., Varma, S., Greenwood, E.A., Christos, P.J., Chao, K.S., Liu, H., Bander, N.H., and Shin, S.J. (2014). Prostate-specific membrane antigen expression in tumor-associated vasculature of breast cancers. APMIS *122*, 482–489. https://doi.org/10.1111/apm.12195.

50. Shen, D., Xie, F., and Edwards, W.B. (2013). Evaluation of phage display discovered peptides as ligands for prostate-specific membrane antigen (PSMA). PLoS One *8*, e68339. https://doi.org/10.1371/journal.pone.0068339.

51. Desmaris, N., Bosch, A., Salaun, C., Petit, C., Prevost, M.C., Tordo, N., Perrin, P., Schwartz, O., de Rocquigny, H., and Heard, J.M. (2001). Production and neurotropism of lentivirus vectors pseudotyped with lyssavirus envelope glycoproteins. Mol. Ther. *4*, 149–156. https://doi.org/10.1006/mthe.2001.0431.

52. Heider, S., Muzard, J., Zaruba, M., and Metzner, C. (2017). Integrated method for purification and single-particle characterization of lentiviral vector systems by size exclusion chromatography and tunable resistive pulse sensing. Mol. Biotechnol. *59*, 251–259. https://doi.org/10.1007/s12033-017-0009-8.

53. Zhang, W., Cao, S., Martin, J.L., Mueller, J.D., and Mansky, L.M. (2015). Morphology and ultrastructure of retrovirus particles. AIMS Biophys. *2*, 343–369. https://doi.org/10.3934/biophy.2015.3.343.

54. Geraerts, M., Willems, S., Baekelandt, V., Debyser, Z., and Gijsbers, R. (2006). Comparison of lentiviral vector titration methods. BMC Biotechnol. *6*, 34. https://doi.org/10.1186/1472-6750-6-34.

55. Sena-Esteves, M., and Gao, G. (2018). Titration of lentivirus vectors. Cold Spring Harb. Protoc. *2018*. https://doi.org/10.1101/pdb.prot095695.

56. Smith-Jones, P.M., Vallabhajosula, S., Navarro, V., Bastidas, D., Goldsmith, S.J., and Bander, N.H. (2003). Radiolabeled monoclonal antibodies specific to the extracellular domain of prostate-specific membrane antigen: preclinical studies in nude mice bearing LNCaP human prostate tumor. J. Nucl. Med. *44*, 610–617.

57. McNamara, J.O., 2nd, Andrechek, E.R., Wang, Y., Viles, K.D., Rempel, R.E., Gilboa, E., Sullenger, B.A., and Giangrande, P.H. (2006). Cell type-specific delivery of siRNAs with aptamer-siRNA chimeras. Nat. Biotechnol. *24*, 1005–1015. https://doi.org/10.1038/nbt1223.

58. Burns, J.C., Friedmann, T., Driever, W., Burrascano, M., and Yee, J.K. (1993). Vesicular stomatitis virus G glycoprotein pseudotyped retroviral vectors: concentration to very high titer and efficient gene transfer into mammalian and nonmammalian cells. Proc. Natl. Acad. Sci. U S A. *90*, 8033–8037.

59. Feili-Hariri, M., Dong, X., Alber, S.M., Watkins, S.C., Salter, R.D., and Morel, P.A. (1999). Immunotherapy of NOD mice with bone marrow-derived dendritic cells. Diabetes *48*, 2300–2308. https://doi.org/10.2337/diabetes.48.12.2300.

60. Looney, B.M., Chernatynskaya, A.V., Clare-Salzler, M.J., and Xia, C.Q. (2014). Characterization of bone marrow-derived dendritic cells developed in serum-free media and their ability to prevent type 1 diabetes in nonobese diabetic mice. J. Blood Disord. Transfus. *5*. https://doi.org/10.4172/2155-9864.1000206.

61. Kong, L., and Sattentau, Q.J. (2012). Antigenicity and immunogenicity in HIV-1 antibody-based vaccine design. J. AIDS Clin. Res. *S8*, 3. https://doi.org/10.4172/2155-6113.

62. Bayon, E., Morlieras, J., Dereuddre-Bosquet, N., Gonon, A., Gosse, L., Courant, T., Le Grand, R., Marche, P.N., and Navarro, F.P. (2018). Overcoming immunogenicity issues of HIV p24 antigen by the use of innovative nanostructured lipid carriers as delivery systems: evidences in mice and non-human primates. NPJ Vaccin. *3*, 46. https://doi.org/10.1038/s41541-018-0086-0.

63. Segura, M.M., Garnier, A., Durocher, Y., Coelho, H., and Kamen, A. (2007). Production of lentiviral vectors by large-scale transient transfection of suspension

cultures and affinity chromatography purification. Biotechnol. Bioeng. *98*, 789–799. https://doi.org/10.1002/bit.21467.

64. Sheu, J., Beltzer, J., Fury, B., Wilczek, K., Tobin, S., Falconer, D., Nolta, J., and Bauer, G. (2015). Large-scale production of lentiviral vector in a closed system hollow fiber bioreactor. Mol. Ther. Methods Clin. Dev. *2*, 15020. https://doi.org/10.1038/mtm.2015.20.

65. Martinez-Molina, E., Chocarro-Wrona, C., Martinez-Moreno, D., Marchal, J.A., and Boulaiz, H. (2020). Large-scale production of lentiviral vectors: current perspectives and challenges. Pharmaceutics *12*. https://doi.org/10.3390/pharmaceutics12111051.

66. Bandeira, V., Peixoto, C., Rodrigues, A.F., Cruz, P.E., Alves, P.M., Coroadinha, A.S., and Carrondo, M.J. (2012). Downstream processing of lentiviral vectors: releasing bottlenecks. Hum. Gene Ther. Methods *23*, 255–263. https://doi.org/10.1089/hgtb.2012.059.

67. Chatalic, K.L., Heskamp, S., Konijnenberg, M., Molkenboer-Kuenen, J.D., Franssen, G.M., Clahsen-van Groningen, M.C., Schottelius, M., Wester, H.J., van Weerden, W.M., Boerman, O.C., and de Jong, M. (2016). Towards personalized treatment of prostate cancer: PSMA I&T, a promising prostate-specific membrane antigen-targeted theranostic agent. Theranostics *6*, 849–861. https://doi.org/10.7150/thno.14744.

68. Serafini, P., Carbley, R., Noonan, K.A., Tan, G., Bronte, V., and Borrello, I. (2004). High-dose granulocyte-macrophage colony-stimulating factor-producing vaccines impair the immune response through the recruitment of myeloid suppressor cells. Cancer Res. *64*, 6337–6343. https://doi.org/10.1158/0008-5472.CAN-04-0757.

69. Dale, D.C., Liles, W.C., Llewellyn, C., and Price, T.H. (1998). Effects of granulocyte-macrophage colony-stimulating factor (GM-CSF) on neutrophil kinetics and function in normal human volunteers. Am. J. Hematol. *57*, 7–15. https://doi.org/10.1002/(sici)1096-8652(199801)57:1<7::aid-ajh2>3.0.co;2-0.